A Non-parametric Method for Landsat-Derived Bathymetry of Northern Alaska Lakes

Geoffroy Heurtier[1,2,3], Jean-Yves Tourneret[1,2,3], Laurent Ferro-Famil[1,4,5], Fanny Larue[6]

[1]University of Toulouse, France, [2]TéSA Laboratory, Toulouse, France, [3]ENSEEIHT-IRIT, Toulouse, France, [4]ISAE-SUPAERO, Toulouse, France, [5]CESBIO, Toulouse, France, [6]CGI, Toulouse, France

***Abstract*—This paper investigates a non-parametric regression approach based on a reproducing kernel Hilbert space framework to model the relationship between Landsat-8 spectral bands and the depth of shallow inland lakes (up to 25m). Unlike existing parametric methods, which rely on predefined assumptions about the relationship between the Landsat bands and the lake depth, the proposed method considers a more flexible non-parametric model based on a radial basis function kernel. This model can handle multiple band ratios to estimate lake depths. The performance of the proposed method is validated on synthetic and real data and compared against traditional parametric models. The results presented in this paper show that the proposed non-parametric model is very competitive in terms of accuracy, while eliminating the need for manual parameter selection, especially in the context of remote sensing of turbid inland water bodies.**

***Index Terms*—Reproducing kernels, Hilbert spaces, Lake Bathymetry, Non-Parametric Modelling, Landsat-8**

I. Introduction

Accurate and consistent monitoring of lakes and reservoirs is essential for improving water management practices. However, such information remains scarce and infrequently shared on a global scale [1]. Satellite data offer interesting potential in this domain, providing an effective solution to address these gaps. Satellite-Derived Bathymetry (SDB) maps underwater topography using satellite imagery, offering a cost-effective and scalable alternative to traditional in-situ methods such as echo sounding. SDB leverages the interaction of visible or infra-red signals with the water column and seafloor to estimate water depth. Initially developed for coastal regions, SDB has shown interesting properties for inland water bodies such as lakes and reservoirs, providing global data coverage through programs such as Landsat and Sentinel-2 [2] [3].

The principle of SDB is to estimate the water depth from water colour using satellite imagery. Estimating the relationship between depth and spectral reflectances requires: (1) depth data, typically obtained through echo sounding to calibrate and validate the models, and (2) spectral data from spaceborne sensors such as Landsat or Sentinel. While SDB offers substantial advantages with respect to in-situ monitoring, its accuracy is influenced by several factors including water turbidity, types of substrate, and assumptions about the relationship between spectral band ratios and water depth. A variety of parametric models have been developed to estimate this relationship, such as the Lyzenga model [4] and the Stumpf model [5] based on the logarithms of the reflectances in blue and green bands. Parametric models usually rely on a simple analytical model for the relationship between reflectance values and water depth using linear, exponential [6], or polynomial [7] functions. However, these approaches have inherent limitations, including their dependence on strict assumptions about the functional form of the relationship and the need for careful parameter tuning. Such constraints can lead to suboptimal performance, particularly in complex aquatic environments with high turbidity or nonlinear depth-colour relationships [8].

This paper presents a non-parametric method adapted to a single or multiple band ratios, which mitigates the bias introduced by assuming a specific functional form between water depth and band ratios. It is organised as follows. Section II presents the parametric models commonly used in the literature for SDB. Section III presents the non-parametric method investigated in this paper with details about the way of estimating its hyperparameters. Real data are then processed in Section IV based on the case study proposed in [6]. The performance of the proposed non-parametric method is evaluated using this dataset. Simulation results show that the proposed method consistently improves the average root mean square error of estimated depths across nearly all lakes, while reducing the need for calibration.

II. Bathymetry estimation using univariate parametric models

This section summarises univariate models that have been considered in the literature for SDB. A univariate model assumes that the depth of a lake at a given pixel only depends on a single band ratio or a log-band ratio. Quantities that have been considered in the literature for SBD are usually based on blue/green, blue/red and green/red band or log-band ratios. These quantities are defined as:

$$g_{\mathrm{r}}(\lambda_a, \lambda_b) = \frac{R(\lambda_a)}{R(\lambda_b)}, \tag{1}$$

$$g_{\mathrm{S}}(\lambda_a, \lambda_b) = \frac{\ln(nR(\lambda_a))}{\ln(nR(\lambda_b))}, \tag{2}$$

with $R(\lambda_a)$ the reflectance of band a. For a given pixel i, the input of the regression model for bathymetry is defined as:

$$x_i = g(\lambda_{a,i}, \lambda_{b,i}), \tag{3}$$

with g refering to either g_{r} or g_{S} depending on the chosen model. A constant term n is classically included in the Stumpf model (2) to ensure the positivity of the terms involved in the ratio (typically $n = 500$), as suggested in [6]. The measured water depth at pixel i is modeled as:

$$z_i = f(x_i; \boldsymbol{w}) + \varepsilon_i, \tag{4}$$

where $x_i \in \mathbb{R}^+$ is defined in (3), ε_i is an additive zero-mean white Gaussian noise, $f(x_i; \boldsymbol{w})$ is a parametric function modeling the relationship between water depth and reflectance ratios and $\boldsymbol{w}$ is a vector of real parameters defining the regression model. This work considers the following parametric models studied in [6] and [7]:

$$f_{\mathrm{l}}(x_i; \boldsymbol{w}) = w_0 + w_1 x_i,\ \boldsymbol{w} = [w_0, w_1]^T, \tag{5}$$

$$f_{\mathrm{q}}(x_i; \boldsymbol{w}) = w_0 + w_1 x_i + w_2 x_i^2,\ \boldsymbol{w} = [w_0, w_1, w_2]^T, \tag{6}$$

$$f_{\mathrm{e}}(x_i; \boldsymbol{w}) = w_0 e^{w_1 x_i},\ \boldsymbol{w} = [w_0, w_1]^T, \tag{7}$$

referred to as linear, quadratic and exponential models. For each model, the parameter vector $\boldsymbol{w}$ can be obtained by minimising a least square cost function defined for a sequence of N observations as:

$$\hat{\boldsymbol{w}} = \arg\min_{\boldsymbol{w}} \sum_{i=1}^{N} [z_i - f(x_i; \boldsymbol{w})]^2. \tag{8}$$

III. A NON-PARAMETRIC BATHYMETRIC MODEL

A parametric model assumes a certain relationship (either linear, quadratic or exponential) between the noiseless band or log-band ratio x_i and the water depth z_i. However, this assumed relationship may not always be correct and the actual relationship can deviate significantly from an assumed standard form. As an example, Fig. 4 shows that the spectro-bathymetric relationship is relatively flat over shallow depths and increases sharply beyond a certain point, which is difficult to describe with a parametric model. Therefore, this paper proposes to investigate a non-parametric model for SDB. Non-parametric models have received a considerable attention in the literature since they are capable of approaching many non-linear and locally smooth relationships between several variables [9]. This section describes the proposed non-parametric regression based on Reproducing Kernel Hilbert Spaces (RKHS).

A. RKHS concept

A kernel k models the similarity between two inputs x_i and x_j belonging to a space denoted as $\mathcal{X}$ using the quantity $k_{ij} = k(x_i, x_j)$. This kernel is called a Mercer kernel if its Gram matrix $\mathbf{K}$ with elements k_{ij} is symmetric $\left(\mathbf{K}^T = \mathbf{K}\right)$ and positive-definite, i.e.,

$$\mathbf{c}^T \mathbf{K} \mathbf{c} \geq 0, \quad \forall \mathbf{c} \in \mathcal{X}.$$

The core idea of kernel methods is that a Mercer kernel can be interpreted as an inner product in a higher-dimensional space, specifically a Hilbert space. According to Mercer's theorem, there exists a mapping ϕ such that:

$$k(x_i, x_j) = \langle \phi(x_i), \phi(x_j) \rangle.$$

This implies that the inputs x_i and x_j can be implicitly projected into a higher-dimensional space as $\phi(x_i)$ and $\phi(x_j)$, and their similarity can be computed in this space using the kernel k, without explicitly calculating ϕ. This concept is known as the kernel trick. As noted in [10], problems that are difficult to solve in lower dimensions often become more manageable in higher dimensions, while the risk of overfitting is minimised. The function f in (4) is expressed as a linear combination of kernel functions associated with N training variables x_i:

$$f(x; \boldsymbol{w}) = \sum_{i=1}^{N} w_i k(x_i, x), \tag{9}$$

where k is the reproducing kernel. An RKHS is a specific Hilbert space containing the function f defined in (9). The kernel k quantifies the similarities between the training point x_i and x so that points that are closer to each other have a stronger influence on the total result. The weights w_i in (9) determine the contribution of each kernel to the function f. The representation of f in this form is guaranteed by the representer theorem, which ensures that the minimiser of a regularised loss function in an RKHS lies in the span of these kernel functions [11]. In particular, a great attention has been devoted to the Gaussian (or radial basis) kernel defined as:

$$k(x_i, x) = \exp\left[-\gamma (x_i - x)^2\right], \tag{10}$$

where the bandwidth parameter γ controls the smoothness of the function f. A small value of γ increases the range of influence for each training point resulting in a smoother and less responsive function f. It is conventional to add a regularisation term to estimate the weight vector $\boldsymbol{w} = (w_1, ..., w_N)^T$, leading to:

$$\hat{\boldsymbol{w}} = \arg\min_{\boldsymbol{w}} \sum_{i=1}^{N} [z_i - f(x_i; \boldsymbol{w})]^2 + \alpha \|\boldsymbol{w}\|^2. \tag{11}$$

This type of regularisation is known as Tikhonov regularisation [12], where the regularisation parameter α balances data fidelity and smoothness regularisation.

B. Univariate regression

Consider N pairs of training data $(x_1, z_1), \ldots, (x_N, z_N)$, where x_i is a feature computed from satellite reflectances using (3) and z_i is the depth of pixel i. The $N \times N$ Gram matrix $\mathbf{K}$ is formed using the elements $k(x_i, x_j)$ in (10) with a fixed parameter γ whose selection is detailed in Section III-D. The weight vector $\boldsymbol{w}$ can be estimated as the solution of the regularised system (11):

$$\hat{\boldsymbol{w}} = \left(\mathbf{K}^T \mathbf{K} + \alpha \mathbf{I}_N\right)^{-1} \mathbf{K}^T \mathbf{z}, \tag{12}$$

where $\mathbf{z} = [z_1, ..., z_N]^T$, $\mathbf{I}_N$ is the $N \times N$ identity matrix, and α is the regularisation parameter. Once the weights have been calculated, a prediction of any new water depth can be determined using a pixel band ratio and (9).

C. Multivariate regression

The regression model introduced in Section III-B can be easily generalised to handle multiple bands or log-band ratios simultaneously. Indeed, the kernel k defined in (10) can be modified as follows:

$$k(\boldsymbol{x}_i, \boldsymbol{x}_j) = \exp\left(-\gamma \|\boldsymbol{x}_i - \boldsymbol{x}_j\|^2\right), \tag{13}$$

where $\boldsymbol{x}_i$ is a vector of band or log-band ratios, e.g.,

$$\boldsymbol{x}_i = [g(\lambda_{b,i}, \lambda_{g,i}), g(\lambda_{b,i}, \lambda_{r,i}), g(\lambda_{g,i}, \lambda_{r,i})]^T,$$

where r, g, b are used for the red, green and blue bands, respectively.

D. Estimation of parameters γ and α

This section first explains how to estimate the bandwidth parameter γ of (10) in order to avoid underfitting (small values of γ) and overfitting (large values of γ). The cross validation method defined in [13] for choosing the correct value of γ consists in minimising the average squared prediction error for leave-one-out predictors. For N training data pairs, the optimal bandwidth parameter is given by:

$$\hat{\gamma} = \arg\min_{\gamma} \frac{1}{N} \sum_{i=1}^{N} [z_i - \hat{f}_{\gamma}^{i}(x_i; \boldsymbol{w})]^2, \tag{14}$$

where $\hat{f}_{\gamma}^{i}$ is the estimator of the function f, built with all the learning dataset except the pair (x_i, z_i) that is left out (Leave-One-Out (LOO) method). Note that a weight $\theta(x_i) = 1_{[x_{l+1}, x_{N-l}]}$ can be introduced in (14), with $l \geq 2$ an integer and $1_{[x_{l+1}, x_{N-l}]}$ the indicator on the interval $[x_{l+1}, x_{N-l}]$ (after sorting the input values x_i in ascending order) to mitigate boundary effects [14].

The parameter α determines the importance given to Tikhonov's regularisation. If α is too small, minimising (11) reverts to the original ill-posed problem and therefore to an instable problem. Conversely, if α is too large, the optimisation primarily minimises $\|\boldsymbol{w}\|^2$, disregarding the data altogether. A trade-off must thus be found between the regularisation terms $\|\boldsymbol{w}\|^2$ and the residue $\sum_{i=1}^{N} [z_i - f(x_i; \boldsymbol{w})]^2$. Such an optimal balance is often identified using the so called L-Curve [15], which plots the residue versus $\|\boldsymbol{w}\|^2$ for different values of α. The optimal value of α corresponds to the inflection point of the L-Curve, i.e., the point where the second derivative changes its sign.

A common approach for selecting both α and γ is a complete grid search, which systematically explores a predefined set of values for each parameter. This method consists of evaluating all possible combinations of α and γ over a discrete grid and selecting the pair that minimises the cross-validation error. This approach is exhaustive and guarantees that the best combination within the predefined grid is found, which explains that it was used in this work. Note however that alternative techniques, such as the Stein's Unbiased Risk Estimate (SURE), could be explored to determine (α, γ) with a reduced computational complexity [16].

IV. Experiments

A. Synthetic Data

The proposed non-parametric model is first evaluated using synthetic data and compared to the parametric models. The blue and green bands from one of the 17 lakes of [6] are first used to create 3 bathymetric maps using the linear, quadratic and exponential Stumpf models defined in (5), (6) and (7). The parameters of each model are chosen so that the resulting depth covers the same range of depths as the original lake (from 1 to 6 meters). The resulting data is sub-sampled such that each interval of depth (from 1 to 2 meters, from 2 to 3 meters, ..) are equally represented. An additive zero-mean Gaussian noise is then introduced with a variance depending on the depth d, precisely $\sigma^2 = a \times d$, an ascending linear function of the water depth. The value of a is set to 0.05, a value visually corresponding to the amount of noise that could be expected in practice.

The generated maps are reconstructed with all the above models including the proposed non-parametric RKHS model (9). These reconstructions are compared to the ground truth, which is available for this synthetic dataset, as shown in Fig. 4. The models are also compared quantitatively via the Root Mean Square Error (RMSE), as shown in Table I. Each set of synthetic data is divided into two equal parts, one used to train the model, the other one used for RMSE computation. In each case, the model that performs the best is the one that was used to create the dataset. However, it can be seen that the proposed non-parametric model performs as well as the best model in all cases. Fig. 1 confirms that the non-parametric model fits the synthetic data better than any other model (the model used to generate the data is not shown for clarity, as it overlaps with the non-parametric model), in agreement with the results in Table I.

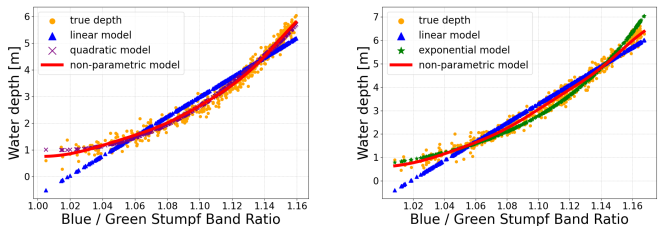

(a) Exponential data. (b) Quadratic data.

Fig. 1: Depth estimation for synthetic exponential and quadratic datasets.

	Models			
Data	Linear	Quadratic	Exponential	RKHS
Linear	0.211	0.211	0.336	0.211
Quadratic	0.302	0.195	0.243	0.195
Exponential	0.379	0.196	0.187	0.187

TABLE I: RMSEs (in meters) of 3 datasets reconstructed with 4 models.

B. Real data

1) Study area

This section considers the in-situ dataset provided by [6], collected across 17 Arctic lakes during a field expedition from July 22 to 27, 2017, using a sonar unit attached to a float plane. The input data are Landsat-8 TOA reflectances from the blue (band 2, 452–512 nm), green (band 3, 533–590 nm), and red (band 4, 636–673 nm) bands, the same observation (LC08_L1TP_077011_ 20160805_ 20170222_01_TI) used in [6]. It is worth noting that Landsat Collection 1 data and products are no longer available for download from the USGS as of December 30, 2022 (https://www.usgs.gov/landsat-missions/landsat-collection-1). Thus the dataset considered in this paper is slightly different from [6]. In order to match the original paper, the dataset consists of L1 data, used without any atmospheric correction, which should be considered for a multi-temporal bathymetric analysis.

2) Training

7 lakes (identified using their IDs provided in Tables II and III) were extracted from the real dataset of [6] to compare the different bathymetric models. The corresponding Landsat-8 images were downloaded from the USGS Explorer. The depth of each pixel was set to the mean of the measured depths located inside the region covered by this pixel, according to the in-situ data provided by [6]. A set of 12 models was created to model the relationship between the satellite image and the lake depth (blue/green, blue/red and red/green band ratios, linear and exponential models, band and log-band ratios, see Section II). Models are indicated in Table II with their type, ratio type and colour bands (e.g., $\mathrm{li}_S(g,r)$ is used for the linear model using the Stumpf ratio of the green and red bands). For each lake, the best parametric model used in [6] was chosen for a more meaningful comparison. Two non-parametric models were then tested, after estimating the bandwidth and regularisation parameters as explained in Section III-D. The first model was built using the band ratio defining the parametric model whereas the second model uses a multiband ratio, as presented in Section III-C.

3) Calibrating γ and α

Parameters γ and α were computed as described in Section III-D. Fig. 2 shows the LOO RMSE corresponding to (14) for different values of γ, which highlights the importance of the bandwidth parameter selection. The U-shaped curve indicates that very small values of γ lead to underfitting, while excessively large values result in overfitting. The optimal value of γ minimises the RMSE, striking a balance between these two effects. If this parameter is suboptimal, results could end up being outperformed by the parametric model, shown in red in Fig. 2. Similarly, Figure 3 displays the L-curve, which is typically used to adjust the regularisation parameter α, as explained in Section III-D. This figure shows the variation of the regularisation term $\|\hat{\boldsymbol{w}}\|$ as a function of the residual norm $\|\mathbf{z}-\mathbf{K}\hat{\boldsymbol{w}}\|$ for different values of α. It illustrates the trade-off between regularisation, which smooths the function, and fidelity to the data. Note that parameters γ and α have been adjusted for each lake, as reflectance values vary significantly across spectral bands.

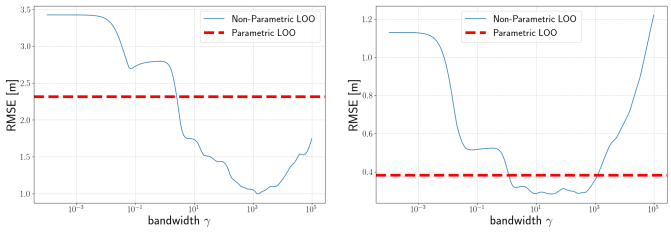

(a) Lake 4199. (b) Lake 3839.

Fig. 2: RMSE of parametric and non-parametric models as a function of the bandwidth parameter γ.

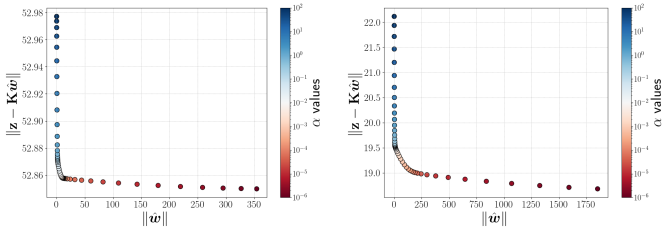

(a) Lake 4199.(γ = 250) (b) Lake 3839. (γ = 35)

Fig. 3: L-Curve for the determination of parameter α.

4) Testing

Training was conducted using 50% of the data whereas the remaining 50% was used for testing. The construction of the training and testing databases was done to ensure that the maximum and minimum depths belong to the training dataset, whereas the second maximum and minimum depths was systematically attributed to the test group. A total of 200 different Monte-Carlo (MC) runs was considered. The average RMSEs computed using these MC runs are reported in Table II. A LOO cross validation (CV) was also performed, which means that for each lake, all the data but one were selected to fit the models, the non-selected vector was used for testing and the results were averaged computing the RMSEs and standard deviations provided in Tables II and III. Table III compares

Lakes			RMSE (meters)		
ID	$D_{\max}$	Model	[6]	Split	LOO
2964	11.7	$\mathrm{li}_S(b,g)$	1.97	2.05	1.61 ± 1.1
3442	1.8	$\mathrm{ex}_r(g,r)$	0.27	0.30	0.18 ± 0.2
3839	5.1	$\mathrm{ex}_r(b,r)$	0.60	0.60	0.38 ± 0.5
4199	8.2	$\mathrm{ex}_r(b,g)$	2.13	2.80	2.31 ± 1.6
4222	8.9	$\mathrm{ex}_r(b,r)$	2.31	2.01	1.74 ± 1.1
4782	2.2	$\mathrm{ex}_S(g,r)$	013	0.15	0.13 ± 0.1
5326	4.4	$\mathrm{ex}_r(b,r)$	0.43	0.52	0.25 ± 0.2

TABLE II: Performance of different parametric models for depth estimation. RMSEs of depth estimates using 50% of the data (Split) and LOO methods.

the RMSEs obtained for the best parametric model and the proposed non-parametric models (univariate and multivariate

Lakes		RMSE (meters)		
ID	$D_{\max}$	Parametric	RKHS One band	RKHS Multiband
2964	11.7	1.61 ± 1.1	1.38 ± 0.8	1.25 ± 0.8
3442	1.8	0.18 ± 0.2	0.18 ± 0.3	0.20 ± 0.3
3839	5.1	0.38 ± 0.5	0.31 ± 0.5	0.35 ± 0.6
4199	8.2	2.31 ± 1.6	1.01 ± 1.5	1.25 ± 1.5
4222	8.9	1.74 ± 1.1	1.71 ± 1.0	1.51 ± 1.2
4782	2.2	0.13 ± 0.1	0.11 ± 0.1	0.11 ± 0.1
5326	4.4	0.25 ± 0.2	0.20 ± 0.3	0.19 ± 0.3

TABLE III: RMSE of depth estimates for parametric and non-parametric regression models (hyperparameters estimated using LOO CV).

regressions) using an LOO CV. These results show the interest of using a non-parametric model, and confirm the results of Section IV-A. Examples of water depth fits obtained using the univariate non-parametric regression are displayed in Fig. 4 for two lakes. The left figure shows that the non-parametric model is the only model in close agreement with the data. The right figure shows that the non-parametric model is able to approximate the exponential shape between the blue/green band ratios and the water depths.

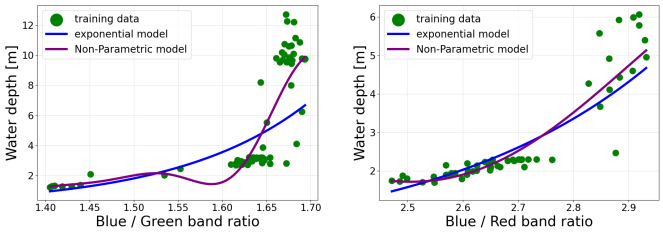

(a) Lake 4199. (b) Lake 3839.

Fig. 4: Examples of functional relationships between band ratios and water depths.

V. Conclusion

This paper investigated a non-parametric model based on kernel methods as an alternative to traditional models for describing the relationship between water depth and the reflectance of different spectral bands of satellite data. A linear combination of kernels appears well-suited for accurately capturing the nonlinear relationship between band/log-band ratios and water depth. The key advantage of non-parametric approaches lies in their flexibility, as they do not impose a predefined functional form for this relationship. This eliminates the need to test multiple functional models and manually select the most effective model for a given lake. While the introduction of a multivariate model does not lead to a significant reduction in RMSEs, it offers the practical benefit of avoiding the selection of the best-performing band ratio for specific conditions.

Different spectral bands provide complementary information about water depth. The blue band is commonly used due to its higher reflectance and lower absorption by water, but it is highly sensitive to atmospheric aerosols. In contrast, red light penetrates only a few meters into the water, making it more relevant for lower depths and turbid waters. Finally, the green band is more effective in clear waters. Leveraging all available spectral information through the proposed multivariate non-parametric model appears to be a robust approach for bathymetry, ensuring greater adaptability across varying water conditions.

It is worth noting that the proposed model can be adapted to specific application needs. For instance, a constraint could be introduced to enforce the bijectivity of the function f. Additionally, a spatial regularisation term could be incorporated into the cost function to encourage smoothness in the estimated depth map. Since band ratios vary significantly between lakes, a separate model was developed for each site. Future research should focus on creating a regional model to mitigate the risk of overfitting while also accounting for time-dependent reflectance variations. Achieving this goal will require integrating additional factors such as atmospheric correction and sunglint removal to improve the proposed bathymetric model.

References

[1] S. Zhang, H. Gao, and B. S. Naz, "Monitoring reservoir storage in South Asia from multisatellite remote sensing," *Water Resources Research*, vol. 50, pp. 8927–8943, Oct. 2014.

[2] A. Arsen, J. F. Cretaux, M. Berge-Nguyen, and R. A. D. Rio, "Remote Sensing-Derived Bathymetry of Lake Poopó," *Remote Sensing*, vol. 6, pp. 407–420, Dec. 2013.

[3] A. Getirana, H. C. Jung, and K. Tseng, "Deriving three dimensional reservoir bathymetry from multi-satellite datasets," *Remote Sensing of the Environment*, vol. 217, pp. 366–374, Nov. 2018.

[4] D. R. Lyzenga, "Passive remote sensing techniques for mapping water depth and bottom features,"

[5] R. P. Stumpf, K. Holderied, and M. Sinclair, "Determination of Water Depth with High-Resolution Satellite Imagery over Variable Bottom Types," *Limnol. Oceanogr.*, vol. 48, pp. 547–556, Jan. 2003.

[6] C. E. Simpson, C. D. Arp, Y. Sheng, M. L. Carroll, B. M. Jones, and L. C. Smith, "Landsat-derived bathymetry of lakes on the Arctic Coastal Plain of northern Alaska," *Earth System Science Data*, vol. 13, p. 1135–1150, Mar. 2021.

[7] F. Eugenio and J. Marcello and A. Mederos-Barrera and F. Marqués, "High-Resolution Satellite Bathymetry Mapping: Regression and Machine Learning-Based Approaches," *IEEE Trans. Geosci. Remote Sensing*, vol. 60, pp. 1–14, Dec. 2021.

[8] C. Wei, Y. Xiao, D. Fu, and T. Zhou, "Impact of Turbidity on Satellite-Derived Bathymetry: Comparative Analysis Across Seven Ports in the South China Sea," *Remote Sensing*, vol. 16, p. 4349, Nov. 2024.

[9] T. Hastie, R. Tibshirani, and J. Friedman, *The Elements of Statistical Learning*. New York: Springer, 2009.

[10] V. N. Vapnik, *The Nature of Statistical Learning Theory*. New York: Springer, 1995.

[11] B. Schölkopf and A. J. Smola, *Learning with Kernels: Support Vector Machines, Regularization, Optimization, and Beyond*. Massachusetts: MIT Press, 2001.

[12] A. N. Tikhonov and V. Y. Arsenin, *Solutions of Ill-Posed Problems*. Washington, D.C.: Vh Winston, 1977.

[13] J. D. Hart and S. Yi, "One-Sided Cross-Validation," *Journal of the American Statistical Association*, vol. 93, pp. 620–631, Jun. 1998.

[14] A. Schindler, *Bandwidth Selection in Nonparametric Kernel Estimation*. PhD thesis, University of Göttingen, Germany, Sep. 2011.

[15] D. Calvetti, S. Morigi, L. Reichel, and F. Sgallari, "Tikhonov regularization and the L-curve for large discrete ill-posed problems," *Journal of Computational and Applied Mathematics*, vol. 123, pp. 423–446, Nov. 2000.

[16] C. M. Stein, "Estimation of the Mean of a Multivariate Normal Distribution," *The Annals of Statistics*, vol. 9, pp. 1135 – 1151, Nov. 1981.